Development and Evaluation of an Autonomous Sensor for the Observation of Sediment Motion*

DONYA FRANK AND DIANE FOSTER

University of New Hampshire, Durham, New Hampshire

PAI CHOU

University of California, Irvine, Irvine, California

YU-MIN KAO

National Tsing Hua University, Hsinchu City, Taiwan

IN MEI SOU

National Research Council Postdoctoral Fellow, Naval Research Laboratory, Stennis Space Center, Mississippi

JOSEPH CALATONI

Marine Geosciences Division, Naval Research Laboratory, Stennis Space Center, Mississippi

(Manuscript received 4 September 2013, in final form 25 December 2013)

ABSTRACT

Measurements within the mobile bed layer have been limited by previous Eulerian-based technologies. A microelectromechanical system device, called a smart sediment grain (SSG), that can measure and record Lagrangian observations of coastal sediments at incipient motion has been developed. These sensors have the potential to resolve fundamental hypotheses regarding the incipient motion of coastal sediments. Angle of repose experiments verified that the sensor enclosure has mobility characteristics similar to coarse gravel. Experiments conducted in a small oscillating flow tunnel verified that the sensors detect incipient motion under various hydrodynamic conditions. Evidence suggests the influence of pressure-gradient-induced sediment motion, contrary to the more commonly assumed bed shear stress criterion. Lagrangian measurements of rotation measured with the newly developed SSG agreed to within 5% of the rotation estimates made simultaneously with high-speed video cameras.

1. Introduction

Characterization of the wave bottom boundary layer (WBBL) hydrodynamics and its impact on sediment transport is integral to understanding coastal processes. The bed shear stresses are used to predict wave energy dissipation and initiation of sediment transport. Incipient motion is the small-scale process that precedes beach and bathymetric changes, potentially impacting navigation and other large-scale processes, including beach erosion and the stability of coastal infrastructure. However, direct measurements of sediment at incipient motion were previously limited to Eulerian observations requiring instruments that were difficult to deploy at the bed without disturbing the flow.

a. Previous efforts

Indirect Eulerian techniques have been used to characterize incipient motion from measurements of flow velocity and bed evolution (Foster et al. 2006; Hanes et al. 2001). Experiments utilizing optical and

* Supplemental information related to this paper is available at the Journals Online website: http://dx.doi.org/10.1175/JTECH-D-13-00180.s1.

Corresponding author address: Donya Frank, Center for Ocean Engineering, University of New Hampshire, 24 Colovos Rd., Durham, NH 03824.
E-mail: donya.frank@unh.edu

DOI: 10.1175/JTECH-D-13-00180.1

acoustic instruments provided insight into the WBBL hydrodynamics and mechanisms triggering incipient motion of sediments. Shields (1936) assessed the impacts of sediment weight and shape on bedload transport at incipient motion in steady flow. He assumed that the force required to move a grain is proportional to its immersed weight. Data suggested that sediment motion results from the destabilizing force of the shear stress exceeding 5% of the immersed weight of the grain, resulting in a critical Shields parameter of 0.05. Numerical models (Davies et al. 1988; Grant and Madsen 1979; Madsen and Wikramanayake 1991; Soulsby and Clarke 2005; Styles and Glenn 2000) and laboratory experiments (Afzalimhr et al. 2007; Huntley and Hazen 1988; Rankin and Hires 2000) also suggest that the bed shear stresses initiate sediment motion.

However, incipient motion has been observed at Shields parameters below the critical threshold in some oscillatory flows (Foster et al. 2006). Pressure-gradient-induced sediment motion may account for the scatter in the Shields diagram and the discrepancies in Shields values at incipient motion. Sleath (1999) quantified the pressure gradient effects with the Sleath parameter S by balancing the inertial and gravitational forces on the grains. Bed mobilizations occurred above a critical $S = 0.29$. Zala Flores and Sleath (1998) observed sediment motion for $S > 0.34$ in an oscillatory flow tunnel. Field observations by Foster et al. (2006) detected sediment motion under peak pressure gradients during the strengthening of onshore flow. Sediment transport was initiated by the large accelerations during flow reversal from offshore to onshore. Sleath values during bed mobilizations yielded a threshold of 0.08–0.1, suggesting a lower critical limit for natural beds exposed to surface gravity waves compared to laboratory experiments with a rigid lid.

Several research efforts have focused on acceleration-driven sediment motion. Terrile et al. (2006) investigated incipient motion of coarse sediments under shoaling waves. They formulated a Shields-like parameter that accounted for acceleration and shear stress to predict motion. Incipient motion occurred between the maximum acceleration and the maximum onshore flow velocity, concurrent with Foster et al. (2006).

Assessing the fluid mechanisms that initiate sediment motion requires direct in situ measurements at the bed. In situ Eulerian measurements of bed-shear stresses have been made with shear plates (Kamphuis 1975; Rankin and Hires 2000). However, they are difficult to deploy in the mobile bed layer and field environments. Other in situ measurements within the WBBL include field observations of velocity with hot-film anemometers (Foster et al. 2000), acoustic Doppler velocimeters (Sherwood et al. 2006; Smyth and Hay 2002), and laser Doppler velocimeters (Trowbridge and Agrawal 1995). Particle image velocimetry (PIV) has been used to observe the fluid–sediment interaction within the WBBL (Earnshaw 1996; Nichols and Foster 2007), but it cannot perform Lagrangian measurements and is difficult to deploy in the field. Moreover, signal attenuation limits measurements within the mobile bed layer. Experiments directly measuring drag and lift forces on grains exposed to steady flow suggest that particle-scale pressure gradients from turbulence also need to be considered (Schmeeckle et al. 2007). More experiments are needed to verify these hypotheses in oscillatory flow, where pressure gradients and instantaneous accelerations are likely to be more significant. Recent advancements in multiaxis force measurement and low-power wireless embedded systems have facilitated the development of a Lagrangian sensor, the smart sediment grain (SSG), that directly measures sediment movement.

b. *Objectives*

The goal is to enhance scientific understanding of the WBBL dynamics by determining the mechanisms that trigger incipient motion. A description of the development of the SSGs as autonomous sensors for the Lagrangian detection of incipient motion under oscillatory flow is presented. They were used to conduct in situ measurements of sediment movement in response to oscillatory forcing to demonstrate their capabilities for capturing incipient motion under waves. In future work, these measurements will be examined in conjunction with PIV velocities to assess the hydrodynamics at incipient motion under various flows and comparisons made with a range of sediment types.

2. The SSG

The SSG consists of a wireless sensor node and a battery inside a water-tight spherical enclosure. The wireless sensor node is a miniature electronic system with sensing, computation, and wireless communication capabilities, termed EcoSD. The node weighs 4 g and measures $2.5 \times 1.5 \times 1.4\ \text{cm}^3$. Each is equipped with two triaxial accelerometers, a flash memory card for onboard data storage, a wireless transmitter integrated with a programmable microcontroller unit (MCU), a chip antenna, and a rechargeable lithium polymer battery, as shown in Fig. 1 (Kao 2012). The accelerometers can be programmed for the range of ± 2, ± 4, or ± 8 times the gravitational acceleration (g), in 12-bit resolution and 1-mg sensitivity. Using two accelerometers to resolve the 6 degrees of freedom for translation and rotation in three dimensions, instead of a gyroscope with an accelerometer, enables the node to be one of the

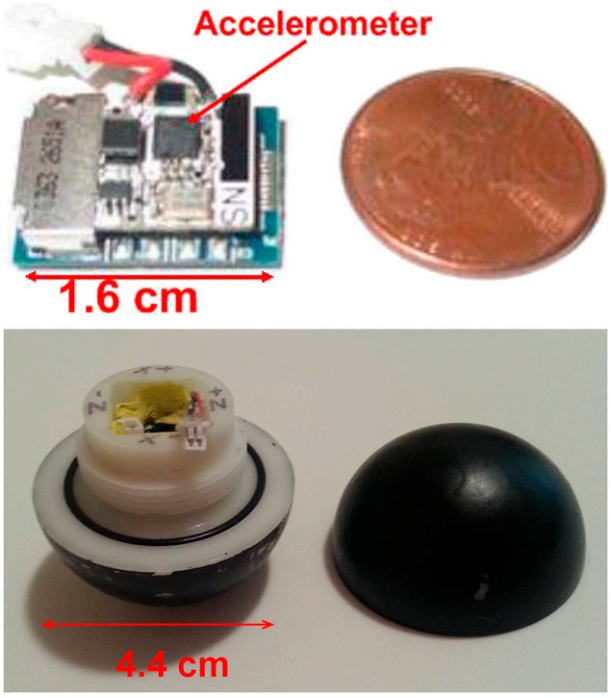

FIG. 1. The SSG. (top) EcoSD node without battery next to penny. (bottom) EcoSD node enclosed in Delrin sphere (painted black).

smallest self-contained programmable inertial measurement units (IMU) (Tsai et al. 2010).

Several enclosures were assessed on their physical and electronic properties, including accuracy, specific gravity, moment of inertia, and radio-frequency transparency. The size and density of the enclosure were scaled based on the mobility criteria for small-scale flumes as specified with the Shields and Sleath parameters. The material options included cored natural granite rocks, acrylic, castable silica ceramic, and Delrin plastic spheres. Delrin was ideal because it was easy to machine, allowed the recharging of the battery with the sensor embedded, had the appropriate density to facilitate tests in the incipient motion regime in small- and large-scale wave flumes, and was transparent to radio frequency. The enclosure diameter is 4.4 cm, comparable to coarse gravel (Fig. 1, bottom). The density of the SSG is approximately $1300\,\mathrm{kg\,m^{-3}}$ with a moment of inertia of $1 \times 10^{-5} \pm 2 \times 10^{-7}\,\mathrm{kg\,m^2}$. The SSGs may not respond exactly like sand grains due to their large size, greater inertia, and lower density—characteristics limited by the design of the electronics package in this generation. However, the SSGs were designed to satisfy the two most relevant scaling laws for the incipient motion regime of interest, Shields and Sleath parameters. The Shields and Sleath parameter formulations inherently account for the sediment density, and therefore the density is not expected to significantly impact the results of the experiments.

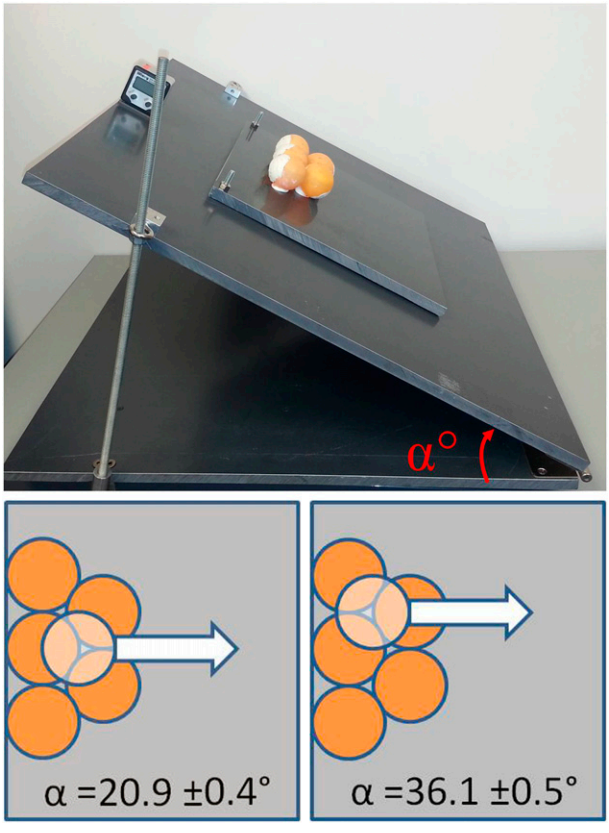

FIG. 2. Experimental setup for the α test, demonstrating top view illustrations of the sediment configurations with mean and standard deviation α values noted. (top) The angle of repose device, (bottom left) sediment configuration A, and (bottom right) sediment configuration B.

3. Evaluation of the SSG

Tests were conducted to determine the noise floor and accuracy of the EcoSD nodes. These tests validated the proper functioning and accurate recording of the accelerations during sediment motion. Time and frequency domain analyses were used to determine the characteristics of the accelerometers. Stationary tests conducted with a commercial reference accelerometer determined a noise floor of $0.5\,\mathrm{m\,s^{-2}}$, low enough to capture the accelerations of sand grains at incipient motion. Calantoni and Puleo (2006) determined that the sediment acceleration at incipient motion was approximately $4\,\mathrm{m\,s^{-2}}$ from modeling sediment grains with a median grain size diameter of 0.0011 m and a density of $2650\,\mathrm{kg\,m^{-3}}$ under sawtooth waves with a period of 6 s and a maximum velocity of $1\,\mathrm{m\,s^{-1}}$. Shaking tests determined that the sensors captured the peak frequency of the oscillations to within 99% and the amplitude to within 90% (see supplementary file JTECH-D-13-00180s1).

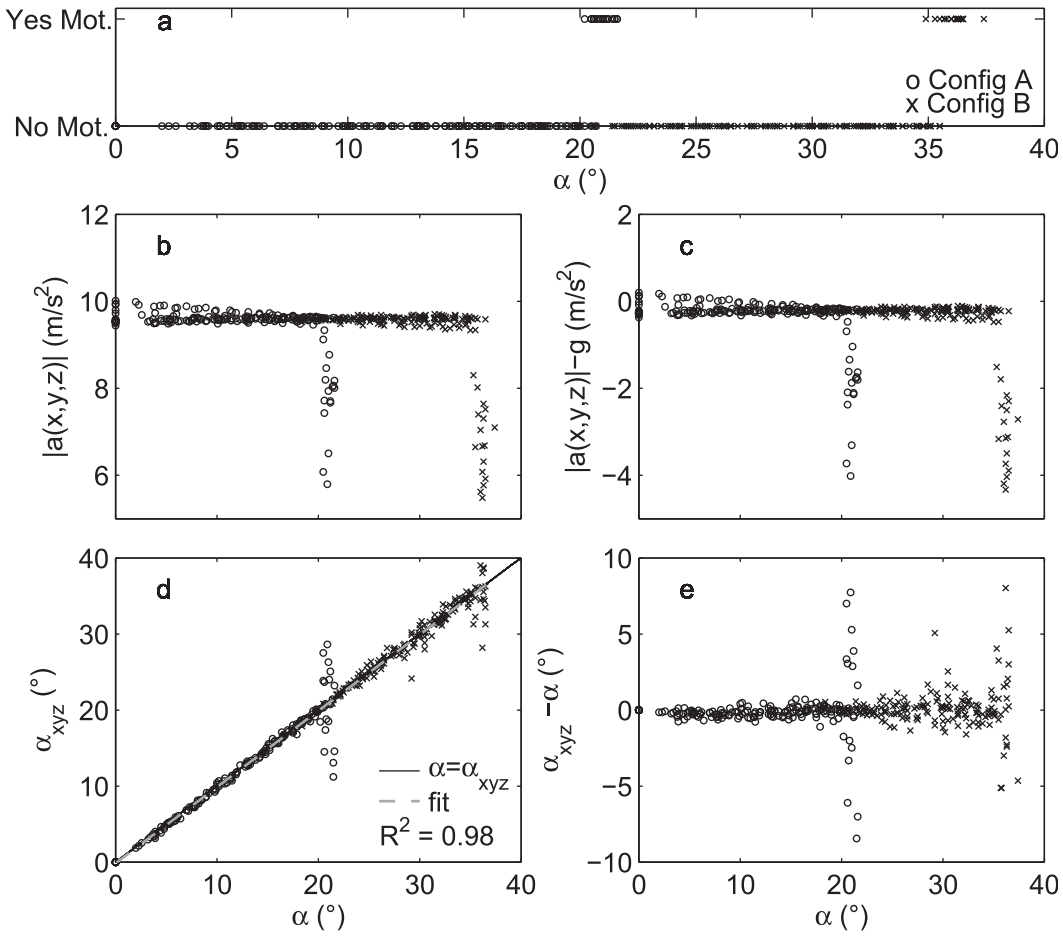

FIG. 3. (a) The α data showing angles of visually observed motion, mean resultant magnitude accelerations measured by the SSG (b) with and (c) without gravity, and angles measured by the SSG (d) at each time step and (e) with the angle of the board removed. A 1:1 ratio line (black) and a trend line (gray) with associated R^2 values are shown in (d).

The angle of repose (α) of the SSG was measured with the device as shown in Fig. 2 (top). Balls similar in size to the SSG were glued in a hexagonally packed manner to the upper board and an angle gauge measured the board angle. The SSG was placed in sediment configuration A (Fig. 2, bottom left). The board was raised incrementally until the SSG rolled between the two balls. The SSG was then placed in configuration B (Fig. 2, bottom right) and the board was raised higher until it rolled over the lower ball. Configuration A resulted in a lower α because there was no ball in front to hinder the movement of the SSG down the slope. The average value and standard deviation were 20.9° ± 0.4°. Data scatter was attributed to small differences in the orientation of the SSG for each trial, suggesting that the center of mass was not exactly in the center of the sphere due to the sensor placement. The reported α for natural sediment with three points of contact is greater, 30° for fine sand and 40° for coarse gravel (Julien 1995). Configuration B resulted in a higher $\alpha = 36.1° \pm 0.5°$, better agreeing with α for coarse gravel. The 10% discrepancy may be due to the SSG being less dense than natural gravel and its perfect spherical shape. Experiments by Van Burkalow (1945) and Miller and Byrne (1966) suggest that the angle of repose would increase with decreased sediment density but decrease with increased size and sphericity. The theoretical α for configurations A and B is 1° lower than the experimental values, 19.5° and 65.3°. The discrepancy was attributed to the uneven distribution of the combined SSG density. The lower α value for configuration A suggests that the direction of the flow relative to the surrounding sediments is important because configuration A would be perceived as configuration B when the flow direction is reversed, as is the case for oscillatory flows.

Figure 3a shows the angles at which motion was visually observed. The measured resultant accelerations by the SSG are approximately equal to the gravitational acceleration, except when the ball moves (Fig. 3b).

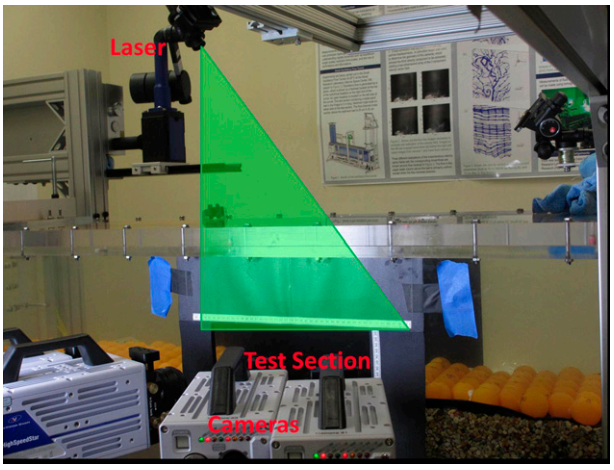

FIG. 4. Experimental setup in the small-oscillating flow tunnel, Naval Research Laboratory, displaying the laser and high-speed cameras of the particle image velocimetry system.

These data are plotted without gravity in Fig. 3c. The accelerations were analyzed to determine the sensor's orientation relative to its initial position (Fig. 3d). This angle correlates well to the angle of the board at each raise, and to α when the ball rolled. A 1:1 ratio and a trend line are shown in black and gray, respectively. The high R^2 value of 0.98 indicates a good fit of the trend line to the data. These data are shown without the trend in Fig. 3e.

4. Oscillating flow tunnel experiments

The SSGs were deployed in the small oscillating flow tunnel at the U.S. Naval Research Laboratory (Fig. 4). Stereographic PIV, composed of four high-speed cameras and a laser, measured velocities from which the shear stresses and pressure gradients will be computed. A range of hydrodynamic conditions were tested with orbital velocity amplitudes from 0.15 to 0.5 m s^{-1} and periods from 2 to 8 s. The fixed SSG bed was packed hexagonally and one freely moving grain was exposed to the flow.

Figure 5 shows PIV images from a sample dataset. The white line across the top of the balls is the laser sheet. The SSG is shown before it moves (Fig. 5a), at the onset of motion (Fig. 5b), during the roll (Figs. 5c–e), and after it has come to rest in the adjacent pocket onshore (Fig. 5f). The equatorial white stripe on the ball was visually tracked to determine the orientation from the PIV images. The initial and present locations of the stripe are indicated by the dashed and solid white lines. The angle between these lines approximates the angle through which the ball has rotated at each time step. The SSG rolls onshore through a maximum angle of 97.2° (Figs. 5b–d) before rolling offshore (Figs. 5d–f) and settling into the adjacent pocket for a final angular displacement of 82°.

The indicated instantaneous free-stream velocities in Figs. 6a–e correspond to images in Fig. 5. Vertical lines indicate incipient motion. Figure 6b shows the accelerations measured by the SSG. As it rolls, the gravity vector rotates from $-x$ to $+z$ direction, in the sensor's reference frame. Figure 6c shows the SSG angle of rotation from its initial orientation based on the measured accelerations. The calculations suggest that the SSG rotates onshore through a maximum angle of 101° before rolling offshore to 82°. These calculations agree within 5% of the rotation angles estimated visually from the images.

Figure 6d shows Shields parameter θ quantifying the bed shear stress effects. The θ_{R98} estimates were based on a time-dependent friction factor formulation (Ribberink 1998) defined as

$$\theta(t) = \frac{\frac{1}{2}\rho f_w |u_\infty(t)| u_\infty(t)}{(\rho_s - \rho) g d_{50}}, \tag{1}$$

where ρ is fluid density, $u_\infty(t)$ is instantaneous velocity above the WBBL, ρ_s is sediment density, d_{50} is median grain size diameter, and f_w, the wave friction factor, was defined as

$$f_w = \begin{cases} \exp\left[5.2\left(\dfrac{k_s}{A}\right)^{0.194} - 5.98\right] & \text{for: } \dfrac{k_s}{A} < 0.63 \\ 0.3 & \text{for: } \dfrac{k_s}{A} \geq 0.63 \end{cases}, \tag{2}$$

where k_s is the Nikuradse roughness ($2.5d_{50}$) and A is the orbital excursion amplitude (Swart 1974). Limitations of the friction factor formulation include the assumption of a constant friction factor throughout the wave cycle and low sensitivity to sediment characteristics such as density and shape. However, it has been shown to provide reasonable estimates of sediment transport parameters at the bed from free-stream velocities. At incipient motion $\theta_{R98} = 0.011$, below the critical threshold of 0.05 (Fig. 6d), suggesting that the bed shear stresses were not responsible for the initiation of motion for the SSG for this flow. Although Ribberink (1998) did not account for the phase lead of the near-bed velocities over the free stream, the spatially averaged phase lead was approximately 17° away from the SSG wake and between 5° and 8° at the height of the ball, and would not account for the sediment motion. Shields parameter estimates were also made with the bed shear stresses based on the drag force, θ_{Fd}. The drag force was computed from the velocities' one-grain diameter upstream of the top of the ball on either side depending on the flow direction and adjusted for time lag to apply these velocities at the SSG.

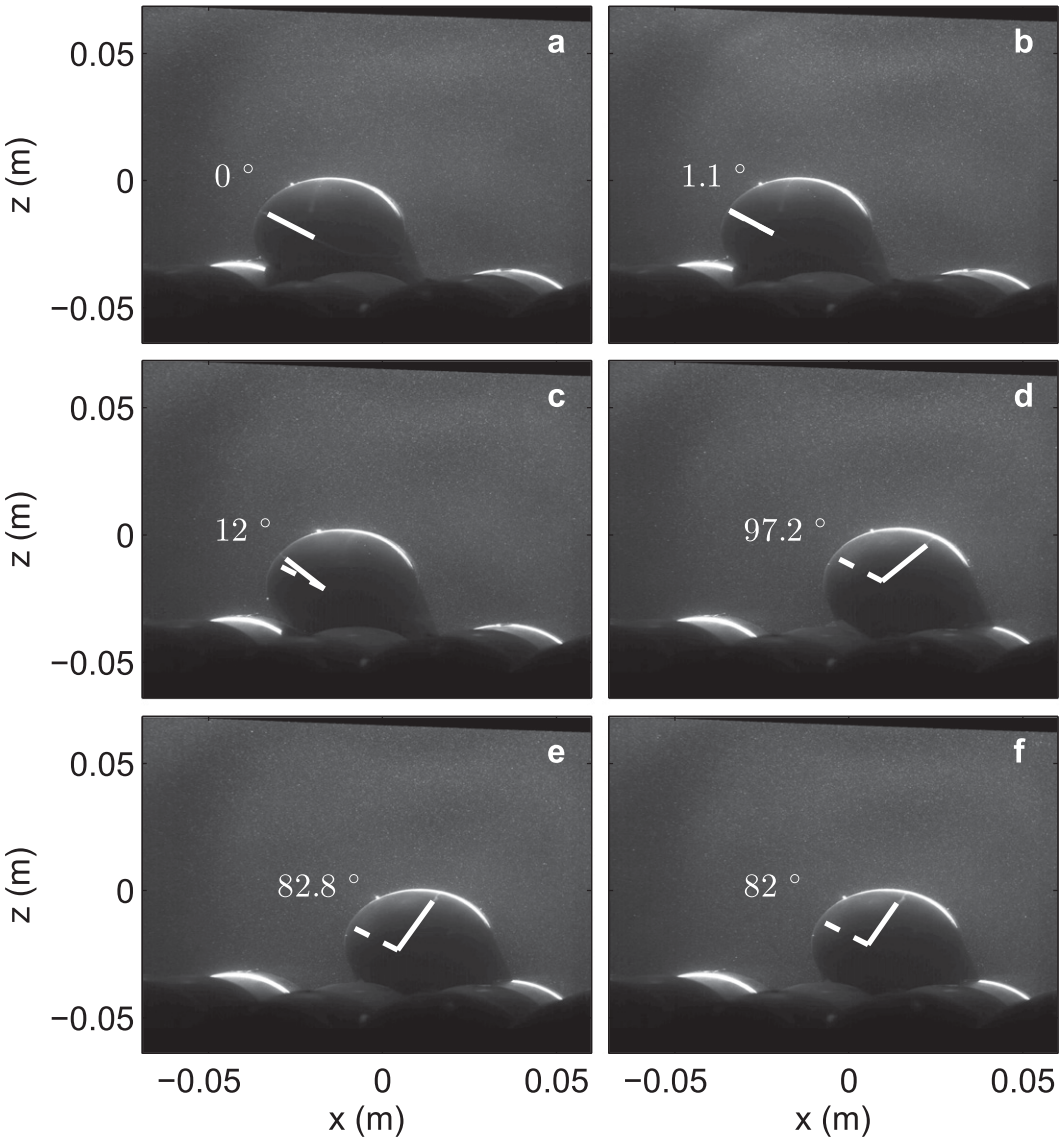

FIG. 5. Snapshots of the SSG during incipient motion. The dashed white line indicates the original position of the white equatorial stripe, and the solid white line indicates the current location at the various times indicated in Fig. 6a. The angle between these lines shown in each panel approximates the angle through which the ball has rotated at each time step.

This process ensures that the deceleration of the flow around the SSG will not affect the calculations of the imposed drag (Schmeeckle et al. 2007). A drag coefficient, $C_D = 0.4$, was used and the shear stresses were computed by dividing the drag force by the projected area of the sphere. The drag force was 0.018 at the onset of sediment motion, well below the critical threshold.

The Sleath parameter, quantifying the pressure gradient effects, is defined as $S = (-\partial P/\partial x)/(\rho_s - \rho)g$, where P is the pressure (Sleath 1999). Linear wave theory approximates the pressure gradients with free-stream accelerations (Foster et al. 2006) $-\partial P/\partial x = \rho[\partial u_\infty/\partial t + u_\infty(\partial u_\infty/\partial x)]$. The onset of motion occurred at $S = 0.1$ during the strengthening phase of the onshore flow, concurrent with Foster et al. (2006) (Fig. 6e). Therefore, incipient motion was triggered by the pressure gradients and not the bed shear stresses for this particular flow.

Foster et al. (2006) suggested a critical threshold for incipient motion, accounting for the combined effects of the bed shear stresses and pressure gradients, $|-\theta d_{50}/h - S| > KC_b(1 + \alpha_c)$, where h is the mobile bed thickness ($=d_{50}$), K is the static coefficient of friction ($=0.38$ for $\alpha = 20.9°$), α_c is a coefficient ($=0$), and C_b is the sediment concentration at the bed ($=0.64$ for a compacted stationary bed) (Sleath 1999); also, $|-\theta - S| = 0.11$ at incipient motion, making $C_b = 0.28$. This lower

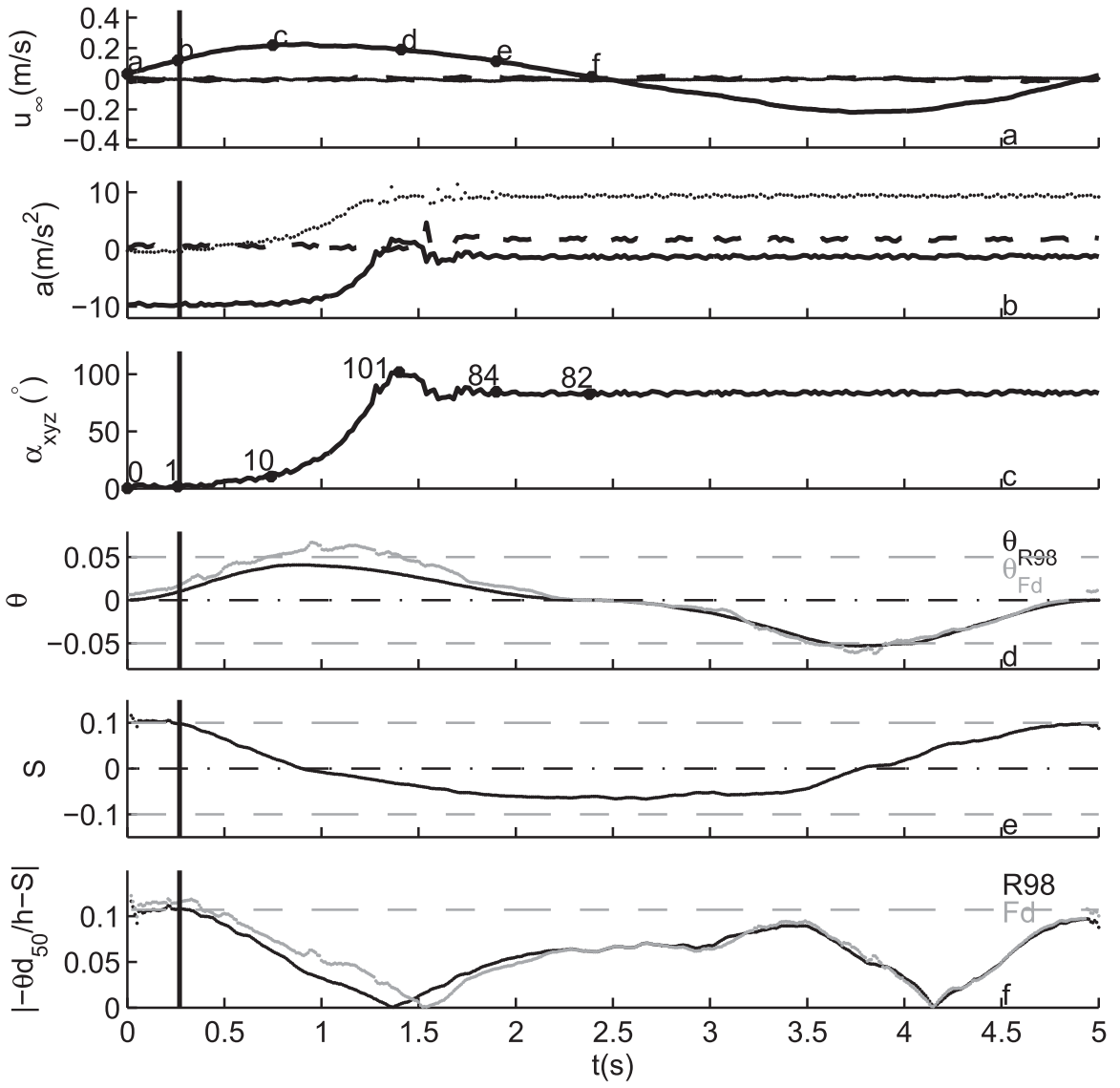

FIG. 6. (a) Free-stream velocities with time amps corresponding to images in Fig. 5, (b) measured accelerations, (c) measured rotation angle by the SSG, (d) θ_{R98} and θ_{Fd}, and (e) S for oscillations with an orbital velocity amplitude of 0.2 m s^{-1} and a period of 5 s. (f) The combined effects of the bed shear stresses and the pressure gradients with θ_{R98} (black) and θ_{Fd} (gray) quantified. The black vertical lines indicate the initiation of SSG motion. In (a),(b), the solid and dashed black lines and the gray lines varying with time represent the x, y, and z directions, respectively. Critical thresholds for the various parameters are indicated by the horizontal dashed gray lines in (d)–(f).

C_b quantifies the differences in the SSG bed configuration with one exposed grain, from that of natural packed gravel. Further investigation is necessary to determine the role of these combined effects and the appropriate critical thresholds for sediment motion.

5. Conclusions

Autonomous sensors were developed to directly measure sediment response to waves. Evaluation of the SSGs verified a low noise floor with enclosures transparent to radio frequency transmission. The angle of repose experiments verified that the mobility of the SSG is comparable to coarse gravel. These results suggested that flow direction relative to the sediment configuration is important in oscillatory flows. Oscillating flow tunnel experiments demonstrated that incipient motion occurred during the strengthening of onshore-directed flow coincident with peaks in the Sleath parameter, suggesting that incipient motion was triggered by the pressure gradients for these flow conditions.

The data indicate that incipient motion in oscillatory flows cannot be fully explained by the bed shear stresses. Further investigation over a broad range of hydrodynamic

conditions, sediment characteristics, and bed configurations is necessary to determine the precise role of the shear stresses, pressure gradients, and the combined effects in initiating sediment motion. Although the SSGs may not respond exactly like sand grains, they were designed to satisfy the two most relevant scaling laws for the incipient motion regime, and the data presented agree very well with the findings of Foster et al. (2006) of pressure-gradient-induced sediment motion of sand in the field. The SSGs represent a breakthrough technology that will help researchers resolve fundamental incipient motion hypotheses used to predict large-scale sediment transport phenomena.

Acknowledgments. This work was sponsored by the National Science Foundation (NSF) under Grants CBET-0933409 and CBET-0933694. Any opinions, or findings are the authors' and may not reflect the views of NSF. In Mei Sou was supported as a postdoctoral fellow through the National Research Council Research Associateship Program at the Naval Research Laboratory (NRL). Joseph Calantoni was supported under base funding to NRL from the Office of Naval Research. Yu-Min Kao was supported by a Ministry of Economic Affairs (Taiwan) Grant 100-EC-17-A-04-S1-044.

REFERENCES

Afzalimhr, H., S. Dey, and P. Rasoulianfar, 2007: Influence of decelerating flow on incipient motion of a gravel-bed stream. *Sadhana,* **32,** 545–559, doi:10.1007/s12046-007-0041-7.

Calantoni, J., and J. A. Puleo, 2006: Role of pressure gradients in sheet flow of coarse sediments under sawtooth waves. *J. Geophys. Res.,* **111,** C01010, doi:10.1029/2005JC002875.

Davies, A. G., R. L. Soulsby, and H. L. King, 1988: A numerical model of the combined wave and current bottom boundary layer. *J. Geophys. Res.,* **93,** 491–508, doi:10.1029/JC093iC01p00491.

Earnshaw, H. C., 1996: A study of flow over a rippled bed using particle image velocimetry. Ph.D. thesis, University of Edinburgh.

Foster, D. L., R. A. Beach, and R. A. Holman, 2000: Field observations of the wave bottom boundary layer. *J. Geophys. Res.,* **105,** 19 631–19 647, doi:10.1029/1999JC900018.

——, A. J. Bowen, R. A. Holman, and P. Natoo, 2006: Field evidence of pressure gradient induced incipient motion. *J. Geophys. Res.,* **111,** C05004, doi:10.1029/2004JC002863.

Grant, W. D., and O. S. Madsen, 1979: Combined wave and current interaction with a rough bottom. *J. Geophys. Res.,* **84,** 1797–1808, doi:10.1029/JC084iC04p01797.

Hanes, D. M., V. Alymov, and Y. S. Chang, 2001: Wave-formed sand ripples at Duck, North Carolina. *J. Geophys. Res.,* **106,** 22 575–22 592, doi:10.1029/2000JC000337.

Huntley, D., and D. Hazen, 1988: Seabed stresses in combined wave and steady flow conditions on the Nova Scotia continental shelf: Field measurements and predictions. *J. Phys. Oceanogr.,* **18,** 347–362, doi:10.1175/1520-0485(1988)018<0347:SSICWA>2.0.CO;2.

Julien, P. Y., 1995: *Erosion and Sedimentation.* 1st ed., Cambridge University Press, 280 pp.

Kamphuis, J. W., 1975: Friction factor under oscillatory waves. *J. Waterw. Port Coastal Ocean Div.,* **101,** 135–144.

Kao, Y.-M., 2012: EcoSTS: A compact and contactless motion measurement system for coastal sediments tracking. M.S. thesis, Dept. of Computer Science, National Tsing Hua University, 66 pp.

Madsen, O., and P. Wikramanayake, 1991: Simple models for turbulent wave-current bottom boundary layer flow. Tech. Rep. DRP-91-1, U.S. Army Corps of Engineers, Coastal Engineering Research Center, 150 pp.

Miller, R. L., and R. J. Byrne, 1966: The angle of repose for a single grain on a fixed rough bed. *Sedimentology,* **6,** 303–314, doi:10.1111/j.1365-3091.1966.tb01897.x.

Nichols, C. S., and D. L. Foster, 2007: Full-scale observations of wave-induced vortex generation over a rippled bed. *J. Geophys. Res.,* **112,** C10015, doi:10.1029/2006JC003841.

Rankin, K. L., and R. I. Hires, 2000: Laboratory measurement of bottom shear stress on a movable bed. *J. Geophys. Res.,* **105,** 17 011–17 019, doi:10.1029/2000JC900059.

Ribberink, J. S., 1998: Bed-load transport for steady flows and unsteady oscillatory flows. *Coastal Eng.,* **34,** 59–82, doi:10.1016/S0378-3839(98)00013-1.

Schmeeckle, M. W., J. M. Nelson, and R. L. Shreve, 2007: Forces on stationary particles in near-bed turbulent flows. *J. Geophys. Res.,* **112,** F02003, doi:10.1029/2006JF000536.

Sherwood, C. R., J. R. Lacy, and G. Voulgaris, 2006: Shear velocity estimates on the inner shelf off Grays Harbor, Washington, USA. *Cont. Shelf Res.,* **26,** 1995–2018, doi:10.1016/j.csr.2006.07.025.

Shields, A., 1936: Anwendung der Anhlichkeitsmechanik und Turbulenzforschung auf die Geschiebebewegung. *Mitt. Preuss. Versuchsanst. Wassebau Schiffbau,* **26,** 20 pp.

Sleath, J. F. A., 1999: Conditions for plug formation in oscillatory flow. *Cont. Shelf Res.,* **19,** 1643–1664, doi:10.1016/S0278-4343(98)00096-X.

Smyth, C., and A. Hay, 2002: Wave friction factors in nearshore sands. *J. Phys. Oceanogr.,* **32,** 3490–3498, doi:10.1175/1520-0485(2002)032<3490:WFFINS>2.0.CO;2.

Soulsby, R. L., and S. Clarke, 2005: Bed shear-stresses under combined waves and currents on smooth and rough beds. HR Wallingford Rep. TR 137, 52 pp. [Available online at tr137_report_richard_repro_smo.pdf.]

Styles, R., and S. M. Glenn, 2000: Modeling stratified wave and current bottom boundary layers on the continental shelf. *J. Geophys. Res.,* **105,** 24 119–24 139, doi:10.1029/2000JC900115.

Swart, D. H., 1974: Offshore sediment transport and equilibrium beach profiles. Delft Hydraulics Laboratory Publ. 131, Delft Hydraulics Laboratory Rep. M918, Part 2, 323 pp.

Terrile, E., A. J. H. M. Reniers, M. J. F. Stive, M. Tromp, and H. Jan Verhagen, 2006: Incipient motion of coarse particles under regular shoaling waves. *Coastal Eng.,* **53,** 81–92, doi:10.1016/j.coastaleng.2005.08.004.

Trowbridge, J. H., and Y. C. Agrawal, 1995: Glimpses of a wave boundary layer. *J. Geophys. Res.,* **100,** 20 729–20 743, doi:10.1029/95JC02131.

Tsai, Y.-L., T.-T. Tu, H. Bae, and P. H. Chou, 2010: EcoIMU: A dual triaxial-accelerometer inertial measurement unit for wearable applications. *Proc. 2010 Int. Conf. on Body Sensor Networks,* Singapore, IEEE, 207–212, doi:10.1109/BSN.2010.47.

Van Burkalow, A., 1945: Angle of repose and angle of sliding friction: An experimental study. *Geol. Soc. Amer. Bull.,* **56,** 669–707, doi:10.1130/0016-7606(1945)56[669:AORAAO]2.0.CO;2.

Zala Flores, N., and J. F. A. Sleath, 1998: Mobile layer in oscillatory sheet flow. *J. Geophys. Res.,* **103,** 12 783–12 793, doi:10.1029/98JC00691.